Materiales de Construcción 75 (358)
April-June 2025, e374
ISSN-L: 0465-2746, eISSN: 1988-3226
https://doi.org/10.3989/mc.2025.381724

Nanosilica synergy: unveiling the strength and fracture mechanisms in advanced concrete composites

J.D. Ríos [a], G. Ruiz [b], D.C. González [c], H. Cifuentes [d]✉, M.A. Vicente [c], R. Yu [b], C. Leiva [e]

a. Department of Mechanical, Energy and Materials Engineering. Escuela de Ingenierías Industriales. Universidad de Extremadura, (Badajoz, Spain)
b. ETSI Caminos, C. y P., Universidad de Castilla-La Mancha, (Ciudad Real, Spain)
c. Department of Civil Engineering, University of Burgos, (Burgos, Spain)
d. Department of Continuum Mechanics and Structural Analysis, Escuela Superior de Ingenieros, Universidad de Sevilla, (Seville, Spain)
e. Department of Chemical and Environmental Engineering, Escuela Superior de Ingenieros, Universidad de Sevilla, (Seville, Spain)
✉: bulte@us.es

Received 10 April 2024
Accepted 2 September 2024
Available on line 30 September 2025

ABSTRACT: This study explores how nanosilica impacts the mechanical properties and fracture behavior of ultra-high-performance concrete (UHPC). We delved into the role of nanosilica in enhancing pozzolanic reactions and its effects on UHPC's pore structure. This was investigated using advanced techniques such as scanning electron microscopy and mercury intrusion porosimetry. We prepared UHPC samples with varying nanosilica concentrations, replacing cement by 0 to 7.5%wt, to understand its influence comprehensively. Our findings reveal that higher nanosilica content, while beneficial in some aspects, compromises the self-compacting nature of UHPC. This necessitated conducting slump tests to evaluate workability. Remarkably, the addition of nanosilica led to a reduction in both capillary and macropores, enhancing the density and strength of the concrete. Specifically, a maximum of 5%wt nanosilica addition resulted in a 13% increase in compressive strength. However, this improvement in strength comes with a trade-off. The fracture energy of UHPC decreased by 23.2%, indicating an increase in brittleness due to nanosilica. Interestingly, tensile strength saw a 10.5% increase, primarily attributed to the enhanced formation of the C-S-H gel, a key component for concrete strength. This study illuminates the dual-edged effects of nanosilica in UHPC, presenting a nuanced view of its role in concrete technology and fracture mechanics.

KEY WORDS: Ultra-high-performance concrete; Nanosilica; Compressive strength; Fracture behavior; Porosimetry; SEM.

Citation/Citar como: Ríos JD, Ruiz G, González DC, Cifuentes H, Vicente MA, Yu R, Leiva C. 2025. Nanosilica synergy: unveiling the strength and fracture mechanisms in advanced concrete composites. Mater. Construcc. 75(358):e374. https://doi.org/10.3989/mc.2025.381724

RESUMEN: *Sinergia de la nanosílice: Desvelando los mecanismos de resistencia y fractura en compuestos de hormigón avanzado.* Este estudio explora cómo el nanosílice afecta las propiedades mecánicas y el comportamiento de fractura del hormigón de ultra alta prestaciones (UHPC). Profundizamos en el papel que el nanosílice juega en la mejora de las reacciones puzolánicas y sus efectos sobre la estructura porosa del UHPC. Para ello, se utilizaron técnicas avanzadas como la microscopía electrónica de barrido y la porosimetría por intrusión de mercurio. Se prepararon muestras de UHPC con diferentes concentraciones de nanosílice, sustituyendo el cemento entre un 0 y un 7,5% en peso, para comprender a fondo su influencia. Nuestros resultados revelan que, aunque un mayor contenido de nanosílice es beneficioso en algunos aspectos, compromete la capacidad autocompactante del UHPC. Esto hizo necesario realizar ensayos de escurrimiento para evaluar su trabajabilidad. Sorprendentemente, la adición de nanosílice llevó a una reducción tanto de los poros capilares como de los macroporos, mejorando la densidad y resistencia del hormigón. Concretamente, una adición máxima del 5% en peso de nanosílice resultó en un aumento del 13% en la resistencia a compresión. Sin embargo, esta mejora en la resistencia conlleva una contrapartida. La energía de fractura del UHPC disminuyó en un 23,2%, lo que indica un aumento en la fragilidad debido al nanosílice. Curiosamente, la resistencia a tracción aumentó en un 10,5%, principalmente

PALABRAS CLAVE: Hormigón de ultra alto rendimiento; Nanosílice; Resistencia a la compresión; Comportamiento a la fractura; Porosimetría; SEM.

1. INTRODUCTION

Concrete stands as the cornerstone of modern infrastructure, forming the backbone of buildings and civil structures globally (1, 2). The pivotal ingredient, cement, however, casts a long shadow on environmental sustainability due to its carbon-intensive production process. Alarmingly, the manufacture of every ton of Portland cement dispatches 0.8 tons of CO2 into our skies (3), contributing to the staggering 4.1 billion tons of annual cement output (4). In response to the escalating concerns over pollution, there has been a global uptick in environmental consciousness, particularly towards slashing CO2 emissions. Illustrating this shift, the European Union has set an ambitious goal of curtailing greenhouse gas emissions by 55% come 2030 (5). This environmental imperative has sparked innovative research into alternative materials with pozzolanic characteristics akin to cement (6–11) These alternatives, which include by-products like silica fume, fly ash, ground granulated blast furnace slag, and limestone powder, not only mimic cement's properties but also offer a pathway to repurpose industrial waste, thus contributing to a more circular economy.

The recent surge in nanotechnology has notably influenced concrete science, particularly through the integration of micro- (12–14) and nano-sized particles (15, 16). These advancements have prompted extensive studies into their effects on concrete's mechanical (1, 17-20) and chemical characteristics (3, 7, 21, 22). Among these, Nanosilica (NS) emerges as a particularly promising addition. This ultrafine material, with particles nearly a thousandfold smaller than those of cement (3), wields a potent chemical profile and expansive specific surface area (23). Such attributes serve as catalysts, multiplying the nucleation sites for cement hydration, thereby enhancing the pozzolanic interactions with portlandite, $Ca(OH)_2$—also known as CH. This process enriches the formation of the calcium silicate hydrate (C-S-H) gel (24, 25), the bedrock of concrete's strength.

The incorporation of NS doesn't just enhance the reaction dynamics; it also leads to a densification of the concrete matrix. As NS particles amalgamate with portlandite, not only is a denser, more robust matrix formed, but the levels of portlandite itself are reduced (26-28). Additionally, the NS particles that remain unreacted act as a filler, occupying the voids within the matrix, which in turn escalates the density and diminishes permeability (3, 18). This intricate interplay between NS and the concrete matrix elevates the material's performance, promising a future where strength and sustainability are no longer mutually exclusive.

While the mechanical fortitude and longevity of concrete enhanced with nanosilica (NS) have been the focus of numerous studies (7, 13, 26, 29-31), the fracture characteristics of NS-augmented ultra-high-performance concrete (UHPC) have not been explored to the same extent. Research to date has revealed that even a modest percentage of NS—ranging from 0.5% to 5%wt—can markedly improve the mechanical behavior of traditional concrete and cement mortars (7, 31-33). Empirical evidence from Li et al. (17) demonstrates a substantial 18% increase in compressive strength at the 28-day mark when 5%wt of NS is incorporated, attributable to the additional C-S-H gel produced and a reduction in the size of $Ca(OH)_2$ crystals. Gadag et al.'s findings align, noting a 21% enhancement in tensile strength in UHPC matrices (29).

Moreover, the nuanced effects of nanosilica (NS) on porosity have been captured by Yu et al., who found that while initial additions of NS can decrease UHPC porosity, beyond a certain threshold, the air content increases, suggesting an optimal NS level contingent on the specific concrete matrix (20, 26, 27, 34). Despite the depth of research into the hydration processes (3, 7, 21) and the quest to improve the interfacial transition zones between aggregate and cement (1, 35) or fiber and cement (16, 17, 25, 36), the full potential of NS in enhancing UHPC's fracture properties remains relatively untapped (12) (37). This underscores the need for a deeper dive into establishing a more comprehensive relationship between NS's influence on the chemical and porosity properties of UHPC and its consequent mechanical and fracture behaviors.

In our investigation, we meticulously explored how varying levels of nanosilica (NS) supplementation, from none to a substantial 7.5%wt, affect the robustness and fracture mechanisms of ultra-high-performance concrete (UHPC). We embarked on a multiscale experimental odyssey, scrutinizing the changes within the concrete matrix. Our toolkit comprised sophisticated mercury intrusion porosimetry (MIP) and scanning electron microscopy (SEM) to dissect the pore architecture and elemental composition. We didn't stop there each UHPC variant was put to the test, undergoing rigorous mechanical and fracture examinations to quantify their strengths and weaknesses.

The crux of our study lies in correlating the intricate details captured by MIP and SEM with the concrete's physical prowess and fracture behavior. By doing so, we aim to decode the intricate dance between the concrete's microstructural alterations spurred by NS additions and their macroscopic mechanical manifestations. This comprehensive analysis strives to uncover the underlying mechanisms that govern the performance of NS-modified concrete, potentially paving the way for more resilient and sustainable infrastructures.

This paper unfolds in a deliberate sequence designed to guide the reader through our investigative journey. Section 2 lays the foundation, detailing the materials selected, the methodologies adopted, and the experimental procedures employed. In Section 3, we delve into the heart of our findings, presenting the results before weaving them into a comprehensive discussion that seeks to both inform and provoke thought. The final section, Section 4, distills our comprehensive analysis into key conclusions, encapsulating the essence of our research and its implications for the future of concrete technology.

2. MATERIALS AND METHODS

2.1. Materials

2.1.1. Material description

In our study, the binder matrix was composed of three main components. First, we utilized Type I cement of the 52.5 R/SR strength class, adhering to the EN 197-1 standard (38), procured from Portland Valderribas. To complement this, silica fume (SF) S-92-D sourced from Sika, and ground-granulated blast-furnace slag (GGBS) provided by Arcelor-Mittal, were incorporated. The aggregate framework consisted of two varieties of quartz sand, each selected for its specific particle size distribution: fine sand (FS) with particles up to 0.315 mm, and a coarser variant (CS) with particles under 0.800 mm. The precise chemical compositions of the binders were determined using X-ray fluorescence spectrometry, the details of which are presented in Table 1.

Table 1. XRF chemical composition of the binder materials (%).

	Cement	GGBS	SF
Al_2O_3	6.59	9.83	0.20
BaO	0.06	—	—
CaO	45.61	35.12	0.30
Cl_2O_3	0.07	—	—
CuO	0.04	—	—
Fe_2O_3	2.85	0.31	0.06
K_2O	1.09	2.01	0.42
MgO	1.00	6.63	0.35
MnO_2	0.05	0.11	—
Na_2O	0.29	0.21	0.12
P_2O_5	0.13	—	—
SiO_2	18.29	27.81	79.58
SO_3	4.02	—	—
SrO	0.05	0.08	—
TiO_2	0.41	0.48	—
ZnO	0.02	—	—

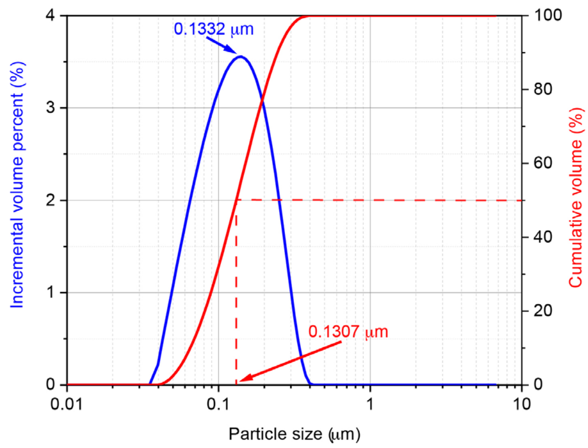

Figure 1. Particle size distribution of nanosilica.

To enhance the concrete's workability, a superplasticizer (20HE) from Sika was introduced. Furthermore, Master-Roc MS 685 nanosilica (NS), supplied by Masterbuilders, was integrated in a carefully measured aqueous solution of 0.250 g/cm³ and a density of 1.134 g/cm³. The specific particle size distribution of this nanosilica, which ranges between 0.040 and 0.398 µm, is graphically detailed in Figure 1. This choice of materials was intended to explore the synergistic potential of traditional and advanced additives in the creation of ultra-high-performance concrete. It is important to clarify that commercial nanosilica material was used following the supplier's instructions, without any prior treatment, to improve the ease of manufacturing the material from a practical standpoint. Therefore, the size distribution is an intrinsic property of the supplied nanosilica and might be considered not to fall within the classification of nanomaterials, but rather submicron materials.

2.1.2. Mixes' composition

Our study engineered six distinct blends of ultra-high-strength concrete (UHSC), each distinguished by varying concentrations of nanosilica (NS) particles used to fortify the mix. The foundational recipe for the matrix remained constant across all variations, as detailed in Table 2. The innovation lay in the substitution of cement with NS at proportions of 0% (creating our baseline reference concrete, NS-0), and escalating additions of 1.5%, 2.5%, 3.5%, 5%, and 7.5%wt for the respective mixes named NS-1.5, NS-2.5, NS-3.5, NS-5, and NS-7.5. Given that NS was introduced in a water suspension form, we meticulously adjusted the water content in each mix to ensure a consistent hydration baseline, crucial for comparing the performance impacts of our NS-enhanced concrete.

Table 2. Constituents and mix compositions of all mixes (kg/m³).

Constituent/mix	NS-0	NS-1.5	NS-2.5	NS-3.5	NS-5.0	NS-7.5
Cement	540	531.9	526.5	521.1	513	499.5
Nanosilica	—	8.1	13.5	18.9	27	40.5
Silica fume	210	210	210	210	210	210
GBFS	310	310	310	310	310	310
FS	470	470	470	470	470	470
CS	470	470	470	470	470	470
Water	204.25	204.25	204.25	204.25	204.25	204.25
Superplasticizer	42	42	42	42	42	42

2.1.3. Mix and sample preparation

Our preparation process began by blending the dry components—cement, silica fume, blast furnace slag, and both fine and coarse aggregates—in a vertical mixer for a duration of four minutes to ensure a uniform dry mix. Following this, we combined the superplasticizer with the nanosilica solution in water and stirred for one minute, creating a homogenous mixture. It's important to note that the water content in the nanosilica solution was accounted for, resulting in each mix having an equal water ratio. The final step was a thorough mixing of all components, solids and liquids alike, for thirty minutes, achieving the desired consistency for our concrete mix.

With the fresh concrete mix ready, we cast three prismatic specimens measuring 40 x 40 x 160 mm³ for each mix type. These were then left to set for 24 hours before being demolded. The curing process, a critical stage for strength development, involved submerging the specimens in water at ambient temperature for a full 28-day cycle.

2.2. Methods

2.2.1. Abrams miniature slump test

To evaluate the workability of our fresh concrete, we employed a bespoke miniature slump test, guided by the principles laid out in the EN 12350-2:2020 standard (39). This method is depicted in Figure 2, where we utilized a scaled-down version of the classic Abrams cone (40), with proportions finely tuned to 50 mm at the top, broadening to 100 mm at the base, and standing 150 mm tall. Each assessment was meticulously carried out on a level surface using a precision-crafted steel mini-slump cone.

The process was simple yet precise: the cone was filled with our freshly mixed concrete and then gently lifted to minimize any inertial influences. A brief ten-second pause post-lifting allowed the concrete to settle, after which we measured the spread in two perpendicular directions. These readings were taken from a bird's-eye view to ensure accuracy.

The average spread of the concrete, denoted as the flow extension (D_f), was the metric of choice to gauge the self-compacting ability of our mix. According to established criteria (41), a concrete mix is deemed self-compacting if its spread falls within the 300 to 400 mm diameter range, a testament to its ability to flow and fill forms under its own weight.

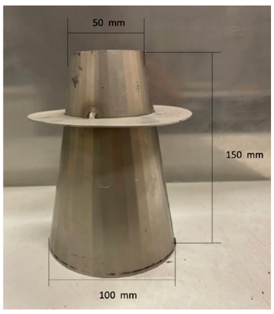

Figure 2. Abrams miniature slump test for fresh concrete.

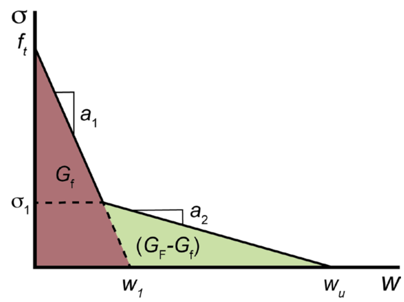

Figure 3. Diagram of a bilinear cohesive law of mixes.

2.2.2. Mercury intrusion porosimetry

To delve into the porosity and pore size intricacies of our ultra-high-strength concrete (UHSC), we employed high-pressure mercury intrusion porosimetry (MIP). This technique allowed us to probe pore structures ranging from the minuscule 1 nm to a more substantial 10 µm. Parameters were meticulously set, with a surface tension of 480 mN/m and a contact angle of 140 degrees, under a formidable pressure of up to 413 MPa. Samples for MIP testing were carefully extracted from the upper segments of our prismatic specimens to ensure consistency and precision in our measurements. Two samples per composition have been subjected to the MIP.

2.2.3. Scanning electron microscopy

Post-mechanical testing, the microscale examination of the UHSC was paramount to understand the material's response to stress. Here, scanning electron microscopy (SEM) came into play, utilizing the high-resolution capabilities of the FEI Teneo microscope. This allowed for an in-depth look at the damage morphology within the fragments of crushed concrete. Selecting fragments that presented flat surfaces, we prepared them for observation by sputter-coating with titanium, thus enhancing the contrast for clearer imaging and meticulous analysis.

2.2.4. Mechanical and fracture tests

Our assessment of the concrete's strength and fracture properties was conducted through rigorous testing of both cubic and prismatic specimens. Prisms were precisely molded to dimensions of 40 × 40 × 160 mm³ while 40 mm³ cubes were obtained by cutting the ends of the prism halves after testing them in bending. The cubic samples were subjected to a compressive strength evaluation in line with the EN 12390-3 standard (42). Meanwhile, the fracture toughness was investigated using three-point bending tests on notched prismatic specimens, adhering to the specifications of the RILEM TCM-85 (43). Each specimen was prepared with a notch-to-depth ratio of 1/6 to ensure uniform stress concentration during testing.

To capture the intricacies of the fracture process, a 10-mm linear vertical displacement transducer was meticulously positioned to record mid-span deflection, coupled with a clip gauge to track the crack mouth opening displacement (CMOD). This measurement was used for regulating the three-point bending tests. The tensile strength, ft, along with other parameters defining the cohesive law (visualized in Figure 3), were extrapolated via an inverse analysis leveraging the non-linear hinge model (44, 45). This analytical approach hinges on fine-tuning the cohesive law parameters to achieve a congruence between the experimental and modeled load-CMOD curves.

For a more granular understanding, the bilinear cohesive law was dissected into two distinct segments (as depicted in Figure 3): the initial branch, G_f, and the subsequent branch, G_F-G_f. The rationale behind this bifurcation of the cohesive law and its implications are thoroughly explored and justified in Section 3.

3. RESULTS AND DISCUSSION

3.1. Abrams miniature slump test

The Abrams slump test outcomes, depicted in Figure 4, reveal a clear pattern: the spread values, indicative of workability, inversely correlate with the increasing nanosilica (NS) content. Each increment of NS introduced to our ultra-high-strength concrete (UHSC) mixes resulted in a measurable dip in spread values, yet all compositions retained self-compacting qualities.

A modest 1.5%wt NS addition marked a 6.7% reduction in spread from the reference concrete (NS-0), setting the stage for a trend where each additional 1% of NS (NS-2.5 and NS-3.5) proportionally lessened spread by around 6%, culminating in decreases of 13.3% and 18.3%, respectively. The impact became more pronounced with 5%wt NS (NS-5), resulting in a 20.8% spread reduction—a significant leap from NS-3.5. This suggests an optimal NS range for workability lies between 3.5% and 5%. The most substantial decrease, however, was seen with NS-7.5, where workability plummeted by 43.3% compared to NS-0, highlighting the consequences of excessive NS—impeded material fluidity due to the NS's high specific surface area which, while enhancing pozzolanic activity through increased water contact, also saps the free water needed for lubrication, thereby curtailing particle movement and spread (46).

In contrast to typical ultra-high-performance fiber concretes (UHPFCs), which exhibit spread values between 25 and 34 cm using the same mini-cone (41), our results demonstrated no signs of aggregate segregation within the spread samples, as evidenced in Figure 5. This finding underscores the delicate balance between nanosilica content and concrete workability, a relationship critical for practical applications of UHSC.

3.2. Mercury intrusion porosimetry

Mercury intrusion porosimetry provided us with a detailed portrait of the pore architecture within our concrete mixes, with a specific focus on NS-0, NS-5, and NS-7.5. The resultant pore size spectrum, ranging from the minute 0.01 µm to the expansive 200 µm, is visually captured in Figure 6. Within this range, the concrete's porosity is characterized by two primary pore types: capillary pores (with a radius of 0.01 to 5 µm, typically the interstitial voids left by water among cement particles) and macropores (larger voids between 5 and 200 µm, mostly formed by entrapped air).

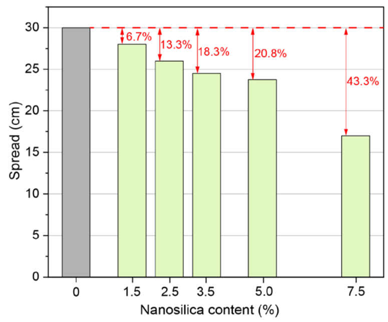

Figure 4. Spread values of each mix with different nanosilica content.

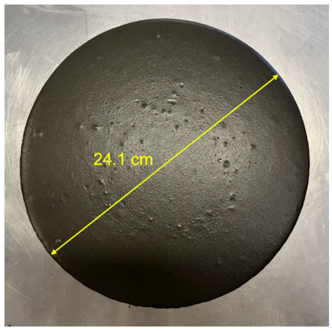

Figure 5. Spread diameter for NS-5.

A delineating green line in Figure 6 neatly segments these two pore realms. NS-0, our reference mix, displayed a predominance of larger macropores peaking at 8 µm, contrasting with fewer capillary pores. Introducing nanosilica to the mix, as seen in NS-5 and NS-7.5, leads to a marked decline in macropore volume (21.8 and 22.5% respectively), as it can be seen in Table 3. This is due to nanosilica's affinity for water, its larger specific surface area, and its role in promoting pozzolanic activity

Interestingly, the NS inclusion raised the count of smaller capillary pores—smaller than 0.5 µm— of 24.2 % with NS-5, especially below 0.04 µm aligning with prior findings (47). Unreacted NS particles, observed within the 0.09 to 0.2 µm range (indicated by orange lines in Figure 6), notably contributed to this effect by occupying potential void spaces.

For the NS-7.5 mix, however, the percentage of pores higher than 8 µm is similar to NS-5 (0.9% lower). The percentage of pores between 0.5 and 8 µm is highest in ND-7.5. In the range between 0.5 and 8 µm, the porosity of NS-7.5 is increased almost double (5,5%), due to the lower workability of the mix (Figure 4). While the percentage of pores lower than 0.5 was slightly lower than NS-5, almost completely disappearing the pores of an NS particle size, this is indicative of poor dispersion at elevated NS levels (48-the synergistic role of micro-nano silica mixture was rarely studied on the direct corrosion protection performance of concrete. This research is to investigate the efficiency of using MS and NS mixture, as cement partial replacement, on corrosion protection and sulphate resistance of cementious materials. In addition, the influence of this silica multi-sized mixture was also studied on some durability characteristics related to corrosion and sulphate protection. Based on the maximum mortar compressive strength, 10% MS and 2% NS were the optimum cement replacement ratios for each size separately. For the comparative purposes, the total cement replacement ratio of MS and NS mixture was kept equal to the optimum MS (i.e.10%50), an insight that underscores the delicate balance between nanoparticle concentration and dispersion within the concrete matrix.

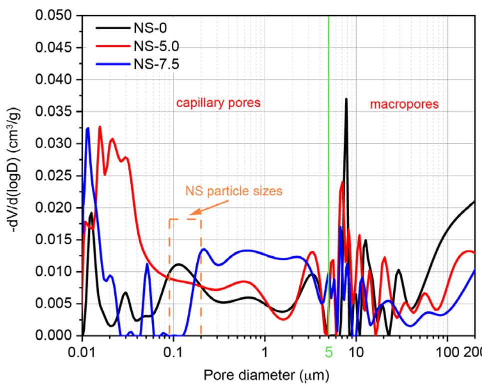

Figure 6. Mercury intrusion porosimetry results.

Table 2. Percentage of Porosity in different ranges of N-0, N-5 and N-0.75.

	DO	N5	N7,5
<0,5 micra	41.7	65.9	62.1
0.5 y 5	8.9	6.5	11.0
>5	49.4	27.6	26.9

3.3. SEM analysis

Through the lens of scanning electron microscopy (SEM), we captured and compared the intricate microstructures of NS-0, NS-0 and NS-7.5 specimens, as vividly presented in Figure 7a, b and c. Figure 7a shows that NS-0 presents a considerable proportion of well-formed plates of calcium hydroxide, which shows that with no NS was added. The SEM imagery brings to light the transformative effect of nanosilica. In NS-5 (Figure 7b), ultra-high-performance concrete with 5 %wt Nano-silica, it can be noted that a very packed structure in the hard sample with a minor number of voids. No calcium hydroxide crystals could be detected. Moreover, finer gels of calcium-silicate-hydrate can be observed, possibly developed from the pozzolan reaction of NS with calcium-hydroxide (51). This tighter lattice is accompanied by an increased and evenly distributed calcium-silicate-hydrate (C-S-H) gel—highlighted at points number 2—bolstering the concrete's inherent strength (Figure 7c).

Unreacted nanosilica particles step into an additional role, filling the microstructural vacancies (52), and thereby augmenting the density of the matrix. In stark contrast, NS-0 samples (Figure 7a) reveal a lesser degree of interconnectivity within the concrete constituents, punctuated by an abundance of pores and void spaces—visible at points number 3.

Nanosilica emerges as a dual-function agent within the concrete mix: a catalyst for pozzolanic reactions that foster the formation of C-S-H gel, and as an infill that mitigates voids, enhancing the overall structural integrity (53). The sample's microstructure with the inclusion of 7.5% NS is displayed in Figure 7(d), in which many pores could be noted. As clarified in Section 3.1., due to the addition of NS significantly diminishing spread (Figure 4) the raising the viscosity of the UHSC, and more free air can be captivated in the sample's matrix.

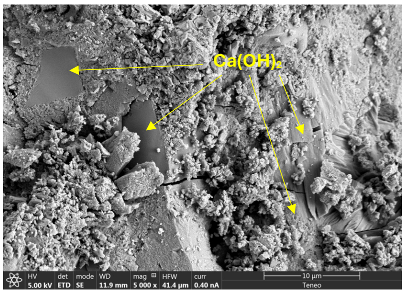

a) NS-0

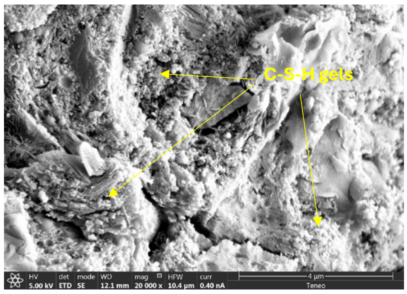

b) NS-5

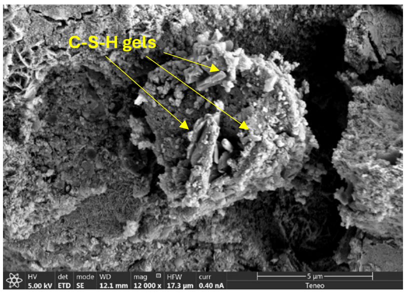

c) NS-5(2)

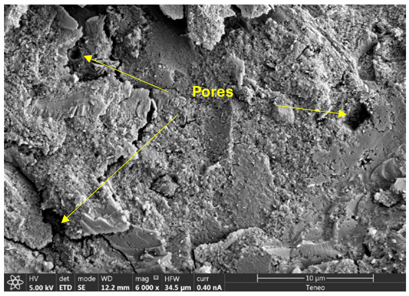

d) NS-7,5

Figure 7. Scanning electron microscopy (SEM) images of reference concrete and nanosilica UHSC. Images of (a) NS-0 and (b) NS-5, (c) NS-5-2 and (d) NS-7.5.

3.4. Mechanical properties

This section unveils the compressive strength across all our concrete mixes, with findings distilled from testing an average of three specimens per mix.

The journey of compressive strength vis-à-vis nanosilica (NS) content is plotted in Figure 8. We observed a crescendo of strength as NS percentages climbed, culminating in a peak 13% increase at 5%wt NS compared to the baseline mix, NS-0. This upward trajectory in strength is attributable to the augmented generation of C-S-H gel, a phenomenon intricately detailed in Section 3.3 and exemplified in Figure 7b. A denser matrix, courtesy of reduced voids and more C-S-H gel, naturally translates to fortified compressive strength (17).

However, surpassing the 5%wt NS threshold (specifically at NS-7.5) triggers a reverse trend, where compressive strength dips to levels akin to NS-1.5. At such high NS levels, the concrete's flowability becomes markedly hampered. The excessive NS hinders even distribution within the matrix, obstructing the full spectrum of pozzolanic reactions and leaving a portion of NS unreacted—an outcome that underscores the delicate balance between NS content and concrete performance.

3.5 Fracture Properties

3.5.1. Size-Independent Fracture Energy

Drawing on the methodology refined by Guinea et al. (54-56), we calculated the size-independent fracture energy using the RILEM work-of-fracture method. Our analysis, derived from three tested samples per mix, is graphically represented in Figure 9. It became evident that as NS content increased, the fracture energy required for the UHPC matrix to fail decreased. Notably, mixtures with 2.5% to 5%wt NS content exhibited fracture energies that were 11%

less than the NS-0 reference, illustrating the trade-off between density and brittleness due to more prevalent C-S-H gel formation (Figure 7) (13, 27). This phenomenon is particularly crucial for UHPCs, which are inherently high-density and often rely on steel fibers to improve ductility and fracture energy (57).

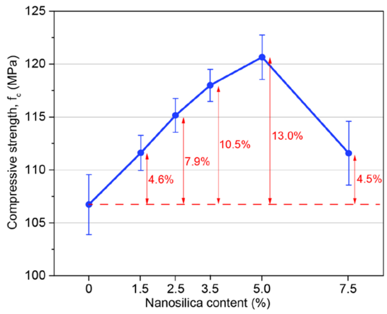

FIGURE 8. Mean compressive strength results for each mix.

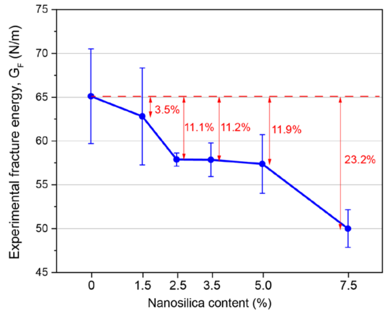

FIGURE 9. Mean experimental size-independent fracture energy of each mix.

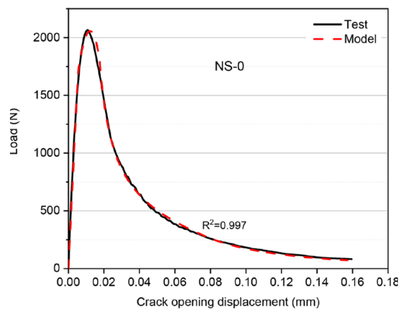

FIGURE 10. Average experimental load-CMOD curves and fitted hinge model: (a) NS0 and (b) NS-3.5.

3.5.2. Cohesive Law Parameters and Tensile Strength

In our quest to decode the fracture mechanics of concrete, we leveraged cohesive law parameters—essential tools for simulating how concrete cracks and understanding the forces at play (54, 58). By employing an inverse approach grounded in the non-linear hinge model (44,namely, the size-independent specific fracture energy G_F, and the corresponding tension softening relation sigma-w (45), we meticulously calculated the bilinear cohesive laws. Our objective was to pinpoint the exact parameters that would align with the experimental load-CMOD curve. Figure 10 illustrates this alignment for mixes with 0 and 3.5% NS content, displaying the impressive accuracy of the fit, with R^2 values very close to unity, underscoring the precision of our inverse analysis.

The data (see Table 3 and Figure 11) reveals a distinct correlation between the NS content and the initial slope of the cohesive law, a_1. Starting from NS-0 with an initial slope of 92 mm^{-1}, there was a general upward trend observed as NS content was increased, indicating a greater material rigidity. This trend was exemplified in mix NS-1.5, reaching 115 mm^{-1}, with a slight dip in NS-2.5 at 102 mm^{-1}, before ascending again in NS-3.5 to 109 mm^{-1}. The most substantial increases were noted in NS-5 and NS-7.5, with initial slopes of 123 mm^{-1} and 139 mm^{-1}, respectively, as detailed in the table provided. This progressive stiffening response up to the onset of microcracking suggests that higher NS contents contribute to a more rigid matrix, which is echoed in the decreased crack opening displacement, signifying a reduced capability to absorb energy during fracture, consistent with the trends observed in measured fracture energy (Figure 9).

A denser matrix, reflected in our MIP results (Figure 6), generally contributes to increased concrete strength due to fewer internal voids. However, it also ushers in a more brittle failure post-peak strength, evidenced by lower fracture energy (13, 59). This was corroborated by tensile strength gains observed with NS supplementation (Table 3 and Figure 12), where NS-5 and NS-7.5 reported increases of 10.5% and 40.4%, respectively. NS-7.5, with the smallest pores, benefited from both the C-S-H gel generation and unreacted NS filling the capillary pores.

3.5.3. Fracture energy consumption

Remarkably, NS-7.5 was found to consume 78.0% of the fracture energy during microcracking (G_f in Table 4), a testament to the mix's high density and the intensive energy required to propagate nano- and microcracks. NS-1.5 to -5 behave very well during the frictional interlocking phase, accounting for 32% on average of the fracture energy consumption (G_F-G_f in Table 4). This suggests that an optimal distribution of NS, resulting in a more uniform C-S-H gel within the matrix, can enhance the ITZ and subsequently increase the energy dissipated during fracture (35, 60).

TABLE 4. Parameters of the bilinear softening diagrams of each mix.

Mix	f_t (MPa)	σ_k (MPa)	a_1 (mm^{-1})	a_2 (mm^{-1})	w_1 (µm)	w_c (µm)	G_F (N/m)	G_f* (%)	G_F-G_f* (%)	E_c (GPa)	ℓ_{ch} (mm)
NS-0	5.7	0.52	92	1.8	11	60	65.2	70.9	29.1	33.0	66
NS-1.5	5.9	0.71	115	3.4	9	43	60.3	67.4	32.6	32.3	56
NS-2.5	6.0	0.70	102	4.6	10	34	55.6	67.2	32.8	35.8	55
NS-3.5	6.0	0.59	109	2.3	9	50	55.5	69.7	30.3	30.4	47
NS-5.0	6.3	0.65	123	2.7	8	46	55.1	67.6	32.4	28.3	39
NS-7.5	8.0	1.55	139	16.4	7	18	48.0	78.0	22.0	38.1	29

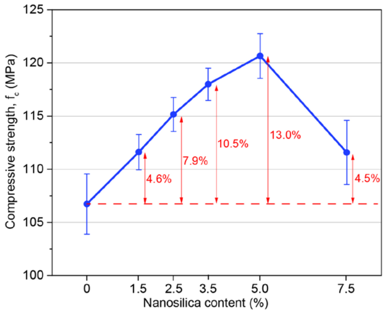

Figure 11. Average bilinear cohesive laws for each mix.

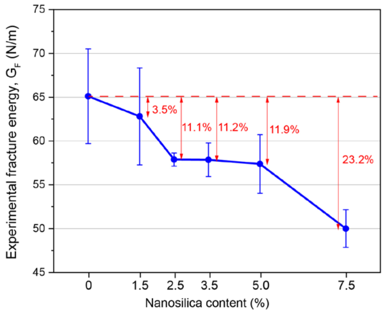

Figure 12. Mean tensile strength results for each mix.

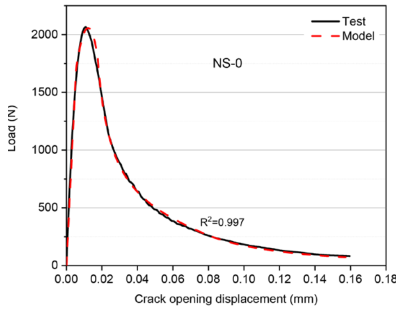

Figure 13. Mean characteristic length results for each mix.

3.5.4. Ductility analysis

In assessing the ductility of our concrete mixes, we turned our attention to the characteristic length (ℓ_{ch} in Table 4)—a parameter intricately tied to the fracture process zone (FPZ). Derived from the product of the elastic modulus and the fracture energy, and inversely related to the square of the tensile strength, the characteristic length serves as a direct indicator of the FPZ's extent and the energy dissipation within it. The NS-0 mix, displaying the highest characteristic length, indicated a larger FPZ and, hence, more energy dissipation, signifying a more ductile behavior (Figure 13). On the contrary, mixes with added NS showed a reduction in characteristic length, reflecting a shorter FPZ and less energy dissipation, which corresponds to a more brittle fracture response—a pattern that is consistent with the lower porosity and reduced fracture energy observed in these mixes (Figure 9).

4. CONCLUSIONS

The comprehensive study conducted on ultra-high-performance concrete (UHPC) with varying concentrations of nanosilica (NS) has culminated in several notable findings:

1. *Workability*: The incorporation of NS into UHPC results in decreased workability, as evidenced by the slump test results. However, the self-compacting nature of the concrete was preserved up to a 5% NS content.
2. *Pore structure*: The mercury intrusion porosimetry revealed that NS modifies the pore structure significantly, reducing macroporosity and altering capillary pore distribution, which directly correlates with the densification of the concrete matrix.
3. *Fracture energy*: The study demonstrated that NS content affects the fracture energy of UHPC, with a notable decrease in fracture energy as NS content increases. Despite this, the highest fracture energy ratio during microcracking was observed with the NS-7.5 mix, indicating a complex interaction between the matrix density and the energy required for crack propagation.
4. *Cohesive law parameters*: Our findings from the cohesive law parameters highlighted that higher NS contents lead to a stiffer initial response in the material up to the point of microcracking. The slope of the initial linear segment of the cohesive law increased with the NS content, suggesting that higher NS levels contribute to a more brittle matrix post-peak strength.
5. *Strength and durability*: The compressive and tensile strength of the concrete mixes increased with the addition of NS, reaching an optimum at 5% NS addition. Beyond this concentration, the effects on flowability and distribution within the matrix negatively impacted the potential for pozzolanic reactions, thereby reducing the overall strength gains.
6. *Ductility*: Characteristic length measurements indicate that NS addition leads to a more brittle behavior, with reduced energy dissipation in the fracture process zone.
7. *Optimization of NS content*: The study underscores the importance of optimizing NS content to balance the benefits of increased strength and density against the adverse effects on workability and fracture energy.

This research provides valuable insights into the design of UHPC mixes with tailored mechanical properties for specific structural applications, promoting a more judicious use of NS to enhance performance while considering practical limitations in construction scenarios.

Acknowledgments

The authors acknowledge the financial support provided to this study by the Spanish Ministry of Science and Innovation (*Ministerio de Ciencia e Innovación*) under projects PID2019-110928RB-C31, -C32 and -C33. PID2023-147971OB-C31, -C32 and -C33.

Authorship contribution statement

José David Ríos: Investigation, Methodology, Validation, Writing – original draft
Gonzalo Ruiz: Formal Analysis, Funding acquisition, Supervision, Writing – review & editing
Dorys Carmen González: Formal Analysis, Investigation, Validation, Writing – review & editing
Héctor Cifuentes: Conceptualization, Formal Analysis, Funding acquisition, Supervision, Writing – review & editing
Miguel Ángel Vicente: Formal Analysis, Funding acquisition, Supervision, Writing – review & editing
Rena C. Yu: Formal Analysis, Investigation, Validation, Writing – review & editing
Carlos Leiva: Conceptualization, Investigation, Methodology, Supervision, Validation, Writing – original draft

Declaration of competing interest

The authors of this article declare that they have no financial, professional or personal conflicts of in-terest that could have inappropriately influenced this work.

REFERENCES

1. Zhang Z, Li Z, He J, Shi X. 2023. High-strength engineered cementitious composites with nanosilica incorporated: Mechanical performance and autogenous self-healing behavior. Cem. Concr. Compos. 135:104837. https://doi.org/10.1016/j.cemconcomp.2022.104837
2. Huseien GF, Shah KW, Sam ARM. 2019. Sustainability of nanomaterials based self-healing concrete: An all-inclusive insight. J. Build. Eng. 23:155–71. https://doi.org/10.1016/j.jobe.2019.01.032
3. Rai S, Tiwari S. 2018. Nano silica in cement hydration. Mater. Today Proc. 5:9196–202. https://doi.org/10.1016/j.matpr.2017.10.044
4. Abdelgader HS, Amran M, Kurpinska M, Mosaberpanah MA, Murali G, Fediuk R. 2022. Sustainable concrete made with ashes and dust from different Sources. Woodhead Publishing Series in Civil and Structural Engineering. 2022:451–479. https://doi.org/10.1016/B978-0-12-824050-2.00003-6
5. European Union. Energy, climate change, environment. https://commission.europa.eu/energy-climate-change-environment_en
6. Kumar Karri S, Rao GVR, Raju PM. 2015. Strength and durability studies on GGBS Concrete. Int. J. Civ. Eng. 2:34–41. https://doi.org/10.14445/23488352/IJCE-V2I10P106
7. Wang X, Hou P, Yu J, Zhou X, Cheng X. 2020. The effects of silica fume on C3A hydration. Constr. Build. Mater. 250:118766. https://doi.org/https://doi.org/10.1016/j.conbuildmat.2020.118766
8. Bahedh MA, Jaafar MS. 2018. Ultra high-performance concrete utilizing fly ash as cement replacement under autoclaving technique. Case Stud. Constr. Mater. 9:e00202. https://doi.org/10.1016/j.cscm.2018.e00202
9. Feng H, Liang J, Guo A, Lv L, Sun Z, Sheikh MN, et al. 2023. Development and design of ultra-high ductile magnesium phosphate cement-based composite using fly ash and silica fume. Cem. Concr. Compos. 137:104923. https://doi.org/10.1016/j.cemconcomp.2022.104923
10. Lin Chan C, Zhang M. 2023. Effect of limestone on engineering properties of alkali-activated concrete: A review. Constr. Build. Mater. 362. https://doi.org/10.1016/j.conbuildmat.2022.129709
11. Dong Y, Liu Y, Hu C. 2023. Towards greener ultra-high performance concrete based on highly-efficient utilization of calcined clay and limestone powder. J. Build. Eng. 66:105836. https://doi.org/10.1016/j.jobe.2023.105836
12. Raza SS, Amir MT, Azab M, Ali B, Abdallah M, El Ouni MH, et al. 2022. Effect of micro-silica on the physical, tensile, and load-deflection characteristics of micro fiber-reinforced high-performance concrete (HPC). Case Stud. Constr. Mater. 17:e01380. https://doi.org/10.1016/j.cscm.2022.e01380
13. Safdar Raza S, Ali B, Noman M, Fahad M, Mohamed Elhadi K. 2022. Mechanical properties, flexural behavior, and chloride permeability of high-performance steel fiber-reinforced concrete (SFRC) modified with rice husk ash and micro-silica. Constr. Build. Mater. 359:129520. https://doi.org/10.1016/j.conbuildmat.2022.129520
14. Patil S, Sudarsana Rao H, Ghorpade VG. 2022. The influence of metakaolin, silica fume, glass fiber, and polypropylene fiber on the strength characteristics of high performance concrete. Mater. Today Proc. 80(2):577-586. https://doi.org/10.1016/j.matpr.2022.11.051
15. Nazar S, Yang J, Amin MN, Khan K, Javed MF, Althoey F. 2023. Formulation of estimation models for the compressive strength of concrete mixed with nanosilica and carbon nanotubes. Dev. Built Environ. 13:100113. https://doi.org/10.1016/j.dibe.2022.100113
16. Dang VP, Kim DJ. 2023. Effects of nanoparticles on the tensile behavior of ultra-high-performance fiber-reinforced concrete at high strain rates. J. Build. Eng. 63:105513. https://doi.org/10.1016/j.jobe.2022.105513
17. Li M, Sun J, Li L, Meng L, Wang S, Wei J, et al. 2023. Effect of nanosilica on fiber pullout behavior and mechanical properties of strain hardening ultra-high performance concrete. Constr. Build. Mater. 367:130255. https://doi.org/10.1016/j.conbuildmat.2022.130255
18. Li G, Liu Q, Niu M, Cao L, Nan B, Shi C. 2020. Characteristic of silica nanoparticles on mechanical performance and microstructure of sulphoaluminate cement/ordinary Portland cement binary blends. Constr. Build. Mater. 242:118158. https://doi.org/10.1016/j.conbuildmat.2020.118158

19. Chithra S, Senthil Kumar SRR, Chinnaraju K. 2016. The effect of colloidal nano-silica on workability, mechanical and durability properties of high performance concrete with copper slag as partial fine aggregate. Constr. Build. Mater. 113:794–804. https://doi.org/10.1016/j.conbuildmat.2016.03.119
20. Varisha, Zaheer MM, Hasan SD. 2021. Mechanical and durability performance of carbon nanotubes (CNTs) and nanosilica (NS) admixed cement mortar. Mater. Today Proc. 42(2):1422–1431. https://doi.org/10.1016/j.matpr.2021.01.151
21. Hou P, Wang X, Zhou X, Cheng X, Shah SP. 2022. Regulations on the hydration, morphology, and sulfate-attack resistivity of C3A with micro/nano-silica particles. Constr. Build. Mater. 324:126388. https://doi.org/10.1016/j.conbuildmat.2022.126388
22. Yu R, Spiesz P, Brouwers HJH. 2014. Effect of nano-silica on the hydration and microstructure development of Ultra-High Performance Concrete (UHPC) with a low binder amount. Constr. Build. Mater. 65:140–50. https://doi.org/10.1016/j.conbuildmat.2014.04.063
23. Khaloo A, Mobini MH, Hosseini P. 2016. Influence of different types of nano-SiO_2 particles on properties of high-performance concrete. Constr. Build. Mater. 113:188–201. https://doi.org/10.1016/j.conbuildmat.2016.03.041
24. Said AM, Zeidan MS, Bassuoni MT, Tian Y. 2012. Properties of concrete incorporating nano-silica. Constr. Build. Mater. 36:838–844. https://doi.org/10.1016/j.conbuildmat.2012.06.044
25. Oh T, You I, Banthia N, Yoo DY. 2021. Deposition of nanosilica particles on fiber surface for improving interfacial bond and tensile performances of ultra-high-performance fiber-reinforced concrete. Compos. Part B Eng. 221:109030. https://doi.org/10.1016/j.compositesb.2021.109030
26. Massana J, Reyes E, Bernal J, León N, Sánchez-Espinosa E. 2018. Influence of nano- and micro-silica additions on the durability of a high-performance self-compacting concrete. Constr. Build. Mater. 165:93–103. https://doi.org/10.1016/j.conbuildmat.2017.12.100
27. Li H, Xiao HG, Yuan J, Ou J. 2004. Microstructure of cement mortar with nano-particles. Compos. Part B Eng. 35:185–189. https://doi.org/10.1016/S1359-8368(03)00052-0
28. Barbhuiya GH, Moiz MA, Hasan SD, Zaheer MM. 2020. Effects of the nanosilica addition on cement concrete: A review. Mater. Today Proc. 32:560–566. https://doi.org/10.1016/j.matpr.2020.02.143
29. Gadag PR, Ghorpade VG, Rao HS. 2022. Evaluation of strength parameters of ultra-fine flyash and nanosilica incorporated High-Performance Concrete. Mater. Today Proc. 49(5):2288–2296. https://doi.org/10.1016/j.matpr.2021.09.344
30. Mobini MH, Khaloo A, Hosseini P, Esrafili A. 2015. Mechanical properties of fiber-reinforced high-performance concrete incorporating pyrogenic nanosilica with different surface areas. Constr. Build. Mater. 101(1):130–140. https://doi.org/10.1016/j.conbuildmat.2015.10.032
31. Sikora P, Rucinska T, Stephan D, Chung SY, Abd Elrahman M. 2020. Evaluating the effects of nanosilica on the material properties of lightweight and ultra-lightweight concrete using image-based approaches. Constr. Build. Mater. 264:120241. https://doi.org/10.1016/j.conbuildmat.2020.120241
32. Ren J, Lai Y, Gao J. 2018. Exploring the influence of SiO_2 and TiO_2 nanoparticles on the mechanical properties of concrete. Constr. Build. Mater. 175:277–285. https://doi.org/10.1016/j.conbuildmat.2018.04.181
33. Shih JY, Chang TP, Hsiao TC. 2006. Effect of nanosilica on characterization of Portland cement composite. Mater. Sci. Eng. A. 424(1,2):266–74. https://doi.org/10.1016/j.msea.2006.03.010
34. Thanmanaselvi M, Ramasamy V. 2021. A study on durability characteristics of nano-concrete. Mater. Today Proc. 80(3):2360-2365. https://doi.org/10.1016/j.matpr.2021.06.349
35. Wang Y, Zeng D, Ueda T, Fan Y, Li C, Li J. 2021. Beneficial effect of nanomaterials on the interfacial transition zone (ITZ) of non-dispersible underwater concrete. Constr. Build. Mater. 293:123472. https://doi.org/10.1016/j.conbuildmat.2021.123472
36. Ren G, Wang J, Wen X, Gao X. 2022. Using sol-gel deposition of nanosilica to enhance interface bonding between sisal fiber and ultra-high performance concrete. Cem. Concr. Compos. 133:104705. https://doi.org/10.1016/j.cemconcomp.2022.104705
37. Atewi YR, Hasan MF, Güneyisi E. 2019. Fracture and permeability properties of glass fiber reinforced self-compacting concrete with and without nanosilica. Constr. Build. Mater. 226:993-1005. https://doi.org/10.1016/j.conbuildmat.2019.08.029
38. EN 197-1:2011. Cement - Part 1: Composition, specifications and conformity criteria for common cements.
39. UNE-EN 12350-2:2020. Testing fresh concrete - Part 2: Slump test.
40. Wedding P, Kantro D. 1980. Influence of water-reducing admixtures on properties of cement paste—a miniature slump test. Cem. Concr. Aggregates. 2(2):95. https://doi.org/10.1520/CCA10190J
41. Nguyen Amanjean E, Mouret M, Vidal T. 2019. Effect of design parameters on the properties of ultra-high performance fibre-reinforced concrete in the fresh state. Constr. Build. Mater. 224:1007–1017. https://doi.org/10.1016/j.conbuildmat.2019.07.284
42. EN-12390-3: 2009. Testing hardened concrete Part 3: Compressive strength of test specimens, AENOR,. Brussels, European Committee for Standarization (CEN): 2009.
43. RILEM TCM-85. 1985. Determination of the fracture energy of mortar and concrete by means of three-point bend tests on notched beams. Mater. Struct. 18:287-290. https://doi.org/10.1007/BF02472918
44. Ramachandra Murthy A, Karihaloo BL, Iyer NR, Raghu Prasad BK. 2013. Bilinear tension softening diagrams of concrete mixes corresponding to their size-independent specific fracture energy. Constr. Build. Mater. 47:1160–1166. https://doi.org/10.1016/j.conbuildmat.2013.06.004

45. Abdalla HM, Karihaloo BL. 2004. A method for constructing the bilinear tension softening diagram of concrete corresponding to its true fracture energy. Mag. Concr. Res. 56(10):597–604. https://doi.org/10.1680/macr.2004.56.10.597
46. Anglade C, Papon A, Mouret M. 2017. Constitutive parameter identification: An application of inverse analysis to the flow of cement-based suspensions in the fresh state from synthetic data. J. Nonnewton. Fluid Mech. 241:14–25. https://doi.org/10.1016/j.jnnfm.2017.01.005
47. Ghafari E, Costa H, Júlio E, Portugal A, Durães L. 2014. The effect of nanosilica addition on flowability, strength and transport properties of ultra high performance concrete. Mater. Des. 59:1–9. https://doi.org/10.1016/j.matdes.2014.02.051
48. Sharkawi AM, Abd-Elaty MA, Khalifa OH. 2018. Synergistic influence of micro-nano silica mixture on durability performance of cementious materials. Constr. Build. Mater. 164:579–88. https://doi.org/10.1016/j.conbuildmat.2018.01.013
49. Erdem S, Hanbay S, Güler Z. 2018. Micromechanical damage analysis and engineering performance of concrete with colloidal nano-silica and demolished concrete aggregates. Constr. Build. Mater. 171:634–642. https://doi.org/10.1016/j.conbuildmat.2018.03.197
50. Shahrajabian F, Behfarnia K. 2018. The effects of nano particles on freeze and thaw resistance of alkali-activated slag concrete. Constr. Build. Mater. 176:172–178. https://doi.org/10.1016/j.conbuildmat.2018.05.033
51. Byung Wan J, Chang Hyun K, Jae Hoon L. 2007. Investigations on the development of powder concrete with nano-SiO_2 particles. KSCE J. Civ. Eng. 11:37–42. https://doi.org/10.1007/BF02823370
52. Behfarnia K, Rostami M. 2017. Effects of micro and nanoparticles of SiO_2 on the permeability of alkali activated slag concrete. Constr. Build. Mater. 131:205–213. https://doi.org/10.1016/j.conbuildmat.2016.11.070
53. Du H, Du S, Liu X. 2014. Durability performances of concrete with nano-silica. Constr. Build. Mater. 73:705–712. https://doi.org/10.1016/j.conbuildmat.2014.10.014
54. Elices M, Guinea GV, Planas J. 1992. Measurement of the fracture energy using three-point bend tests: Part 3- Influence of cutting the P-δ tail. Mater. Struct. 25:327-334. https://doi.org/10.1007/BF02472591
55. Planas J, Elices M, Guinea G V. 1992. Measurement of the fracture energy using three-point bend tests: Part 2-Influence of bulk energy dissipation. Mater. Struct. 25:305-312. https://doi.org/10.1007/BF02472671
56. Guinea GV, Planas J, Elices M. 1992. Measurement of the fracture energy using three-point bend tests: Part 1- Influence of experimental procedures. Mater. Struct. 25:212–218. https://doi.org/10.1007/BF02473065
57. Ríos JD, Leiva C, Ariza MP, Seitl S, Cifuentes H. 2019. Analysis of the tensile fracture properties of ultra-high-strength fiber-reinforced concrete with different types of steel fibers by X-ray tomography. Mater. Des. 165:107582. https://doi.org/10.1016/j.matdes.2019.107582
58. Al-Azzawi BS, Karihaloo BL. 2017. Flexural fatigue behavior of a self-compacting ultrahigh performance fiber-reinforced concrete. J. Mater. Civ. Eng. 29(11):04017210. https://doi.org/10.1061/(ASCE)MT.1943-5533.0002051
59. Zheng Y, Zhuo J, Zhang P. 2021. A review on durability of nano-SiO2 and basalt fiber modified recycled aggregate concrete. Constr. Build. Mater. 304:124659. https://doi.org/10.1016/j.conbuildmat.2021.124659
60. Bahmani H, Mostofinejad D. 2022. Microstructure of ultra-high-performance concrete (UHPC) – A review study. J. Build. Eng. 50:104118. https://doi.org/10.1016/j.jobe.2022.104118